Physics Letters A 375 (2011) 3834–3839

Contents lists available at SciVerse ScienceDirect

Physics Letters A

www.elsevier.com/locate/pla

Preparation and tomographic reconstruction of an arbitrary single-photon path qubit

So-Young Baek [a,b,*], Yoon-Ho Kim [a]

[a] Department of Physics, Pohang University of Science and Technology (POSTECH), Pohang, 790-784, Republic of Korea
[b] Department of Electrical and Computer Engineering, Fitzpatrick Institute for Photonics, Duke University, Durham, NC 27708, USA

ARTICLE INFO

Article history:
Received 11 July 2011
Received in revised form 22 August 2011
Accepted 23 August 2011
Available online 22 September 2011
Communicated by P.R. Holland

Keywords:
Quantum information
Quantum communication
Quantum state engineering

ABSTRACT

We report methods for preparation and tomographic reconstruction of an arbitrary single-photon path qubit. The arbitrary single-photon path qubit is prepared losslessly by passing the heralded single-photon state from spontaneous parametric down-conversion through variable beam splitter. Quantum state tomography of the single-photon path qubit is implemented by introducing path-projection measurements based on the first-order single-photon quantum interference. Using the state preparation and path-projection measurements methods for the single-photon path qubit, we demonstrate preparation and complete tomographic reconstruction of the single-photon path qubit with arbitrary purity.

1. Introduction

The basic unit of quantum information is the qubit, a two-dimensional quantum system. Quantum computing and quantum communication protocols base their operation on preparation, manipulation, and measurement of multiple qubits [1,2]. In photonic quantum information research, various photonic degrees of freedom such as, polarization [3], spatial modes [4], orbital angular momentum [5], time of arrival of a photon [6], etc. can be used to implement the qubit.

The spatial degree of freedom of a photon, in particular, has attracted much attention in recent years because it is comparatively easy to implement the qubit or the qudit, a D-dimensional quantum system [5,7–14]. The spatial mode of a photon also enables preparation of single-photon multi-qubit states when combined with other degrees of freedom, such as polarization [15–20].

Spatial qubits or qudits have usually been generated with the transverse spatial profiles of the photon pairs from spontaneous parametric down-converted (SPDC) by selecting the angular momentum eigenstate [5,7–9], by choosing discrete regions in the transverse profile [10,14], or by sending photons through multiple slits [11,12].

These methods, however, generally produce the spatial qubits or qudits in the pure state.[1] Also, in the double-slit/multiple-slit based qubit/qudit preparation schemes, the loss of photon flux is unavoidable and the diffraction effect causes poor beam mode, making it difficult for long-distance transmission. Furthermore, accessing the superposition bases, which is necessary for quantum state tomography, is difficult for the spatial qubit/qudit prepared by using a double-slit/multiple-slit. For instance, the projection measurement in the superposition basis was implemented by using free evolution of the spatial qubits [22] or by performing measurements in the focal and image planes of a lens [23,24]. High-fidelity and high-efficiency state preparation and tomographic reconstruction of the spatial qubit/qudit are thus difficult if prepared by using a double-slit/multiple-slit [25,26].[2]

Therefore, for quantum information applications of the spatial qubit/qudit (e.g., linear optical quantum computing, quantum teleportation, quantum cryptography, etc.), developing simpler and efficient methods of state preparation (not only pure states, but also mixed states) and tomography is essential. On the one hand, the ability to prepare the spatial qubit/qudit with arbitrary purity

* Corresponding author at: Department of Electrical and Computer Engineering, Fitzpatrick Institute for Photonics, Duke University, Durham, NC 27708, USA. Tel.: +19196605156; fax: +19196605247.
E-mail address: soyoungb@gmail.com (S.-Y. Baek).

0375-9601/$ – see front matter
doi:10.1016/j.physleta.2011.08.064

[1] In Ref. [21], the spatial qubit mixture was prepared by using an incoherent mixture of two laser beams that pump the SPDC process. This method, however, is rather limited in the range of states it can prepare.

[2] Recently, in Ref. [25] and Ref. [26], measurement strategy of spatial qubit/qudit by using programable multipixel liquid-crystal displays instead of mechanical slits were introduced. The methods may reduce the drawbacks of the previous double-slit/multiple-slit based qubit/qudit preparation schemes.

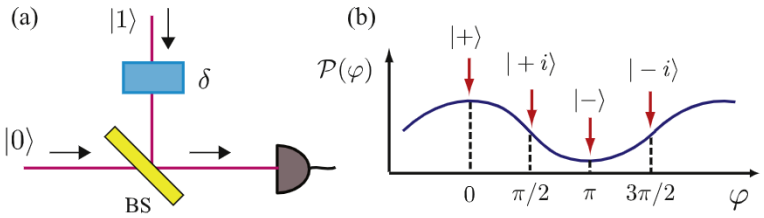

Fig. 1. (a) Schematic diagram of a single-photon path projector. A phase shifter (δ) and a 50/50 beam splitter (BS) enable the path qubit projection measurement on an arbitrary basis state $|b\rangle = (|0\rangle + e^{i\varphi}|1\rangle)/\sqrt{2}$ (b) The probability that the detector will click due to the single-photon path qubit, $\mathcal{P}(\varphi)$, depends on the phase φ included in a projection basis. Especially φ=0, $\pi/2$, π, and $3\pi/2$ correspond to projection basis $|+\rangle$, $|+i\rangle$, $|-\rangle$, and $|-i\rangle$, respectively. Note $\varphi = \delta + \pi/2$.

would allow us to experimentally study the impact of the quantum state purity loss to various quantum information protocols in, for example, quantum key distribution [27–29], quantum circuits [30], quantum cloning [31], and quantum error correction [32]. On the other hand, multi-qubit/multi-qudit mixed states can be used for classifying entanglement. For instance, certain mixed quantum states are known to have bound entanglement which is not distillable by local operation and classical communication [33]. Also, a careful examination between entanglement and entropy for mixed states lead to the so-called maximally entangled mixed state, which carries the maximum amount of entanglement possible for a given mixedness [34].

In this paper, we demonstrate methods to prepare an arbitrary single-photon spatial qubit and to perform full tomographic characterization of the prepared spatial qubit. The spatial qubit with arbitrary purity is implemented as the superposition/mixed state of a single-photon occupying two output modes of a variable beam splitter [15–18]. To perform quantum state tomography, we introduce path projection measurement (analogous to polarization projection measurement) where the path projector (analogous to the polarization projector-polarizer) is made of a phase shifter and a 50/50 beam splitter. Using the state preparation and path projection measurement methods for the single-photon spatial qubit, we experimentally demonstrate high-fidelity preparation and tomographic reconstruction of single-photon path qubit with arbitrary purity.

2. Path projection measurements and tomography

In order to characterize the mixed state qubit as well as the pure state qubit, quantum state tomography, a statistical method of reconstructing the quantum state density matrix based on a set of projection measurement outcomes, is necessary. The first step to quantum state tomography of the single-photon spatial qubit is to define the set of projection operators.

Let us define the projection operator on a single-photon path qubit as

$$P_m = |m\rangle\langle m|, \tag{1}$$

where the projection basis states necessary for quantum state tomography are given as

$$\{|m\rangle\} = \{|0\rangle, |1\rangle, |+\rangle, |-\rangle, |+i\rangle, |-i\rangle\}. \tag{2}$$

Here we define $|0\rangle$ and $|1\rangle$ as the computational basis states of a single-photon path qubit: $|0\rangle$ is for the horizontal path and $|1\rangle$ is for the vertical path, see Fig. 1(a). The superposition states of the single-photon path qubits are defined as follows: $|+\rangle \equiv (|0\rangle + |1\rangle)/\sqrt{2}$, $|-\rangle \equiv (|0\rangle - |1\rangle)/\sqrt{2}$, $|+i\rangle \equiv (|0\rangle + i|1\rangle)/\sqrt{2}$, and $|-i\rangle \equiv (|0\rangle - i|1\rangle)/\sqrt{2}$. Note that these six particular measurement basis states correspond to eigenstates of the Pauli operators: $\hat{\sigma}_z$, $\hat{\sigma}_x$, and $\hat{\sigma}_y$.

Fig. 1(a) shows a schematic diagram of a single-photon path projector. We use a phase shifter (δ) and a 50/50 beam splitter (BS) to implement path projective operator measurements on an arbitrary measurement basis state $|\psi\rangle$,

$$|\psi\rangle \equiv \frac{1}{\sqrt{2}}\left(|0\rangle + e^{i\varphi}|1\rangle\right), \tag{3}$$

where $\varphi = \delta + \pi/2$ and $\pi/2$ is the additional phase due to the beam splitter reflection.

Two paths sharing a single-photon will constructively or destructively interfere at the beam splitter, see Fig. 1(a), depending on the value of φ. Fig. 1(b) shows the relation between the probability, $\mathcal{P}(\varphi)$, that the detector in Fig. 1(a) will click as a function of φ. Four projective operation measurements on the basis $|+\rangle$, $|+i\rangle$, $|-\rangle$, $|-i\rangle$ are then realized by setting φ to 0, $\pi/2$, π, and $3\pi/2$, respectively. In Fig. 1(b), the path qubit is assumed to be prepared in $|\psi\rangle = |+\rangle$, so the detection probability $\mathcal{P}(\varphi)$ has the maximum value for $\varphi = 0$ and the minimum value for $\varphi = \pi$.

While the first-order single-photon quantum interference is needed to implement the path projector for the superposition basis states $|\psi\rangle$ shown in Eq. (3), the projection operators for computational basis states $P_0 = |0\rangle\langle 0|$ and $P_1 = |1\rangle\langle 1|$ require direct detection without interference. For example, to perform the projection measurement on a basis state $|0\rangle$, we detect the single-photons coming from path 0 only by simply blocking path 1. In this case, the count rate at the detector in Fig. 1(a) will show no interference fringes and the count rate at the detector will be reduced by half due to the 50/50 BS. Thus, the detected count rate is doubled to obtain the measurement outcome corresponding to the projection basis $|0\rangle$. The path projection measurement on the computational basis state $|1\rangle$ can be done similarly.

The set of six measurement outcomes $n_{(m)}$ of the single-photon detector, which is directly proportional to the detection probability $\mathcal{P}(|m\rangle)$, allows linear tomographic reconstruction of the single-photon path qubit density matrix. The reconstructed density matrix by the linear tomography method, however, sometimes violate the physical properties of a density matrix. To avoid this problem, the maximum likelihood method was applied as follows [35,36]. First, we generate a physical density matrix which satisfies the normalization condition, Hermiticity, and positivity, as a function of six variables. And then we introduce the "likelihood function" which quantifies how good physical density matrix is in relation to the experimental data. Finally, using standard numerical optimization techniques, we obtain the best estimate of the density matrix by maximizing the likelihood function.

The experimentally reconstructed density matrix ρ_{exp} is compared to the theoretically expected density matrix ρ_{theory} which is determined by the intended settings of the experimental setup. The fidelity $F = (Tr\sqrt{\sqrt{\rho_{theory}}\rho_{exp}\sqrt{\rho_{theory}}})^2$ is then calculated to see how closely the two density matrices overlap and the state purity is analyzed by calculating $Tr(\rho_{exp}^2)$. For single qubits, the linear entropy S_L is defined as $S_L(\rho_{exp}) = 2(1 - Tr(\rho_{exp}^2))$, which ranges from 0 for a pure state to 1 for a completely mixed state [34].

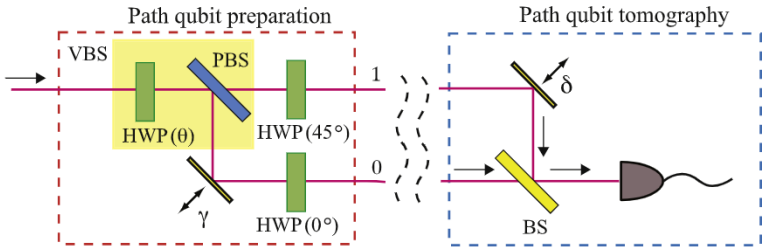

Fig. 2. Schematic of the experiment. Path qubit preparation: The single-photon path qubit is prepared with a heralded single-photon state from spontaneous parametric down-conversion and a variable beam splitter (VBS), which consists of a half wave plate (HWP) and a polarizing beam splitter (PBS). Path qubit tomography: The prepared path qubit is tomographically characterized by the path projective operator measurements introduced in Fig. 1. Note that while the variable beam splitter in path qubit preparation part is used to split a single path into two paths, the beam splitter in the path qubit tomography part is used to combine two paths into one. See the text for details.

3. Experiment

The experimental setup to prepare and characterize the single-photon path qubit is shown in Fig. 2. To prepare the single-photon state, we employ the heralded single-photon state, conditionally prepared by detecting the trigger photon of the photon pair born in the process of spontaneous parametric down-conversion (SPDC) [19,37–39]. A 3 mm thick type-I β-barium borate (BBO) crystal was pumped by a 408 nm cw diode laser (48 mW), generating a pair of collinear frequency-degenerate entangled photons centered at 816 nm via the SPDC process. The pump beam was focused on the BBO crystal with a $f = 300$ mm lens and the pump beam waist at the BBO was roughly 80 μm. The co-propagating photon pairs were then separated spatially by using a 50/50 beam splitter. After passing through two interference filters, centered at 816 nm with 10 nm FWHM bandwidth, the SPDC photons were coupled into single-mode optical fibers using ×10 objective lenses located at 600 mm from the crystal. The idler photon was directly coupled to the trigger detector so that the detection signal can be used to herald the single-photon state for the signal photon.

The signal photon, at the output of the fiber collimator, is prepared in the vertical polarization, $|V\rangle$, by using a fiber polarization controller and a vertical polarizer. To prepare an arbitrary single-photon path qubit, the vertically polarized single-photon is injected into a variable beam splitter (VBS) which consist of a half wave plate (HWP) and a polarizing beam splitter (PBS), see Fig. 2. Two HWPs after the PBS ensure that the photons at 0-path and 1-path have the same polarization. The spatial phase γ of a path qubit is introduced by moving the mirror. Especially, for $\gamma = 0$ (modulo 2π), we obtain the single-photon path qubit in the pure state given as

$$|\psi\rangle = \alpha|0\rangle + \beta|1\rangle, \tag{4}$$

where α and β are experimentally determined by the HWP angle θ of the VBS. The prepared path qubit is experimentally characterized by performing path qubit tomography which require the outcomes of the path projection measurements $n_{(m)}$, where m is listed in Eq. (2).

4. Single-photon path qubit: preparation and tomography

For preparing a pure state path qubit, the preparation and tomography stages in Fig. 2 together must form an equal-path Mach–Zehnder interferometer [15]. We first set the HWP angle to $\theta = 22.5°$ to prepare the pure state path qubit in the state $|\psi\rangle = \frac{1}{\sqrt{2}}(|0\rangle + |1\rangle) = |+\rangle$. To perform the path projective measurements on the superposed basis $|+\rangle$, $|+i\rangle$, $|-\rangle$, $|-i\rangle$, the mirror in tomography part was scanned around the balanced position of the Mach–Zehnder interferometer. Here we measure the coincidence counts between the trigger detector and the signal detector, since we use a heralded single-photon state as the single-photon source.

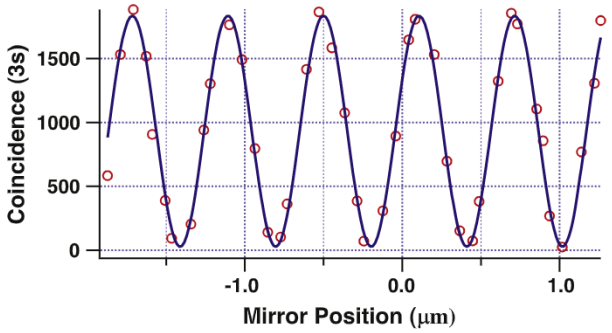

Fig. 3. The first-order singe-photon quantum interference for the pure state path qubit. The HWP angle of the VBS is set at $\theta = 22.5°$ to prepare $|\psi\rangle = |+\rangle$.

Fig. 3 shows the first-order single-photon interference that exhibits the relation between the triggered signal counts versus the mirror position, which determines the phase φ included in the path projection basis of Eq. (3). For the prepared path qubit $|\psi\rangle = |+\rangle$, the interference fringe shows about 97% visibility. The maximum and the minimum coincidence counts corresponds to the measurement outcome $n_{(+)}$ and $n_{(-)}$, respectively. The measurement outcomes $n_{(+i)}$ and $n_{(-i)}$ can also be obtained from Fig. 3. The projection measurement outcome for the computational basis state $|0\rangle$ ($|1\rangle$) was obtained by doubling the coincidence count measured by blocking the path 1 (0).

Note that 100% visibility can be obtained only for the pure state path qubit satisfying $|\alpha| = |\beta|$. As the difference between $|\alpha|$ and $|\beta|$ increases, the visibility of the single-photon interference will decreases. In particular, for the path qubit prepared in the computational basis $|0\rangle$ or $|1\rangle$, the interference fringe will completely disappear.

The experimentally reconstructed density matrices for the pure state single-photon path qubit are shown in Fig. 4. The results show clearly that it is possible, with ease, to prepare high-purity single-photon path qubits with high fidelity.

Let us now discuss how to prepare and characterize a mixed state path qubit. One of the easiest method to add mixedness in the path qubit is to increase distinguishablity between two spatial modes $|0\rangle$ and $|1\rangle$ by adding a large phase factor γ, comparable with the coherence time of the single-photon state.

Fig. 5(a) shows the first-order single-photon interference observed at the output of the Mach–Zehnder interferometer. The HWP angle at the VBS is set at $\theta = 22.5°$ in this experiment so that the prepared single-photon path qubit has the same probability of being in path 0 and in path 1. To prepare the pure state path qubit, the delay γ introduced by the mirror should be very small around $x = 0$ μm. The mixed state path qubit can then be prepared by

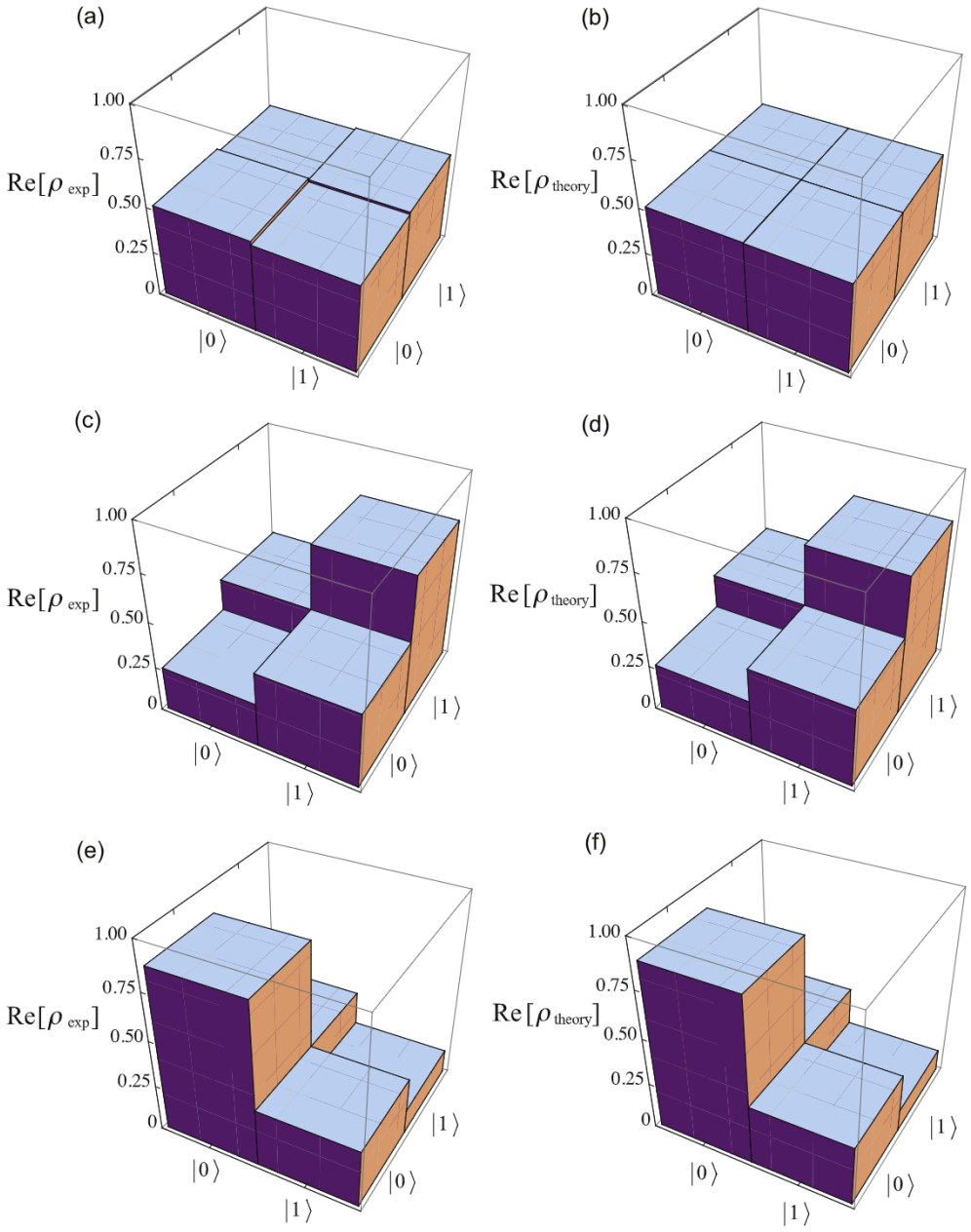

Fig. 4. Real parts of the experimentally reconstructed (ρ_{exp}) (a) and the theoretically expected (ρ_{theory}) (b) density matrices for a HWP setting $\theta = 22.5°$. The calculated fidelity is $F = 0.984$ and the state purity is $Tr(\rho_{exp}^2) = 0.970$. (c) and (d) show ρ_{exp} and ρ_{theory} for $\theta = 30°$. (e) and (f) are the results for $\theta = 10°$. For these angle settings, we obtain $F = 0.988$, $Tr(\rho_{exp}^2) = 0.978$ and $F = 0.983$, $Tr(\rho_{exp}^2) = 0.968$, respectively.

adding a much larger γ value and, in this experiment, we chosethe following three mirror positions: $x_1 = -10$ μm, $x_2 = -40$ μm, and $x_3 = -80$ μm. The experimental results for these three cases are shown in Fig. 5(b), Fig. 5(c), and Fig. 5(d), respectively.

As shown in Fig. 5(b)–Fig. 5(c), when the Mach–Zehnder interferometer is balanced within the coherence length of the signal photon, the mixed state path qubit exhibits some partial coherence between two computation basis states $|0\rangle$ and $|1\rangle$ and its density matrix has non-zero off-diagonal terms. As the Mach–Zehnder interferometer gets more unbalanced, i.e., the mixedness increases, the amplitudes of the off-diagonal terms decrease. Finally, when the Mach–Zehnder interferometer gets completely unbalanced, the off-diagonal terms become almost zero, see Fig. 5(d). From these data, it is apparent that the mixedness in the single-photon path qubit is related directly to the reduction of interference visibility. By changing the HWP angle setting at the VBS and the mirror position, it is possible to prepare an arbitrary path qubit.

5. Conclusion

We introduced a simple method to prepare an arbitrary single-photon path qubit with the heralded single-photon state from spontaneous parametric down-conversion and a variable beam splitter. Compared to the spatial qubits, generated by sending photons through multiple pixels or slits, our path qubit can be prepared without any spatial filtering and thus it can be implemented with high photon flux and good spatial modes.

To characterize the prepared spatial qubit, we introduced the projection measurement scheme for the single-photon path qubit in which the projection measurement outcomes are directly ob-

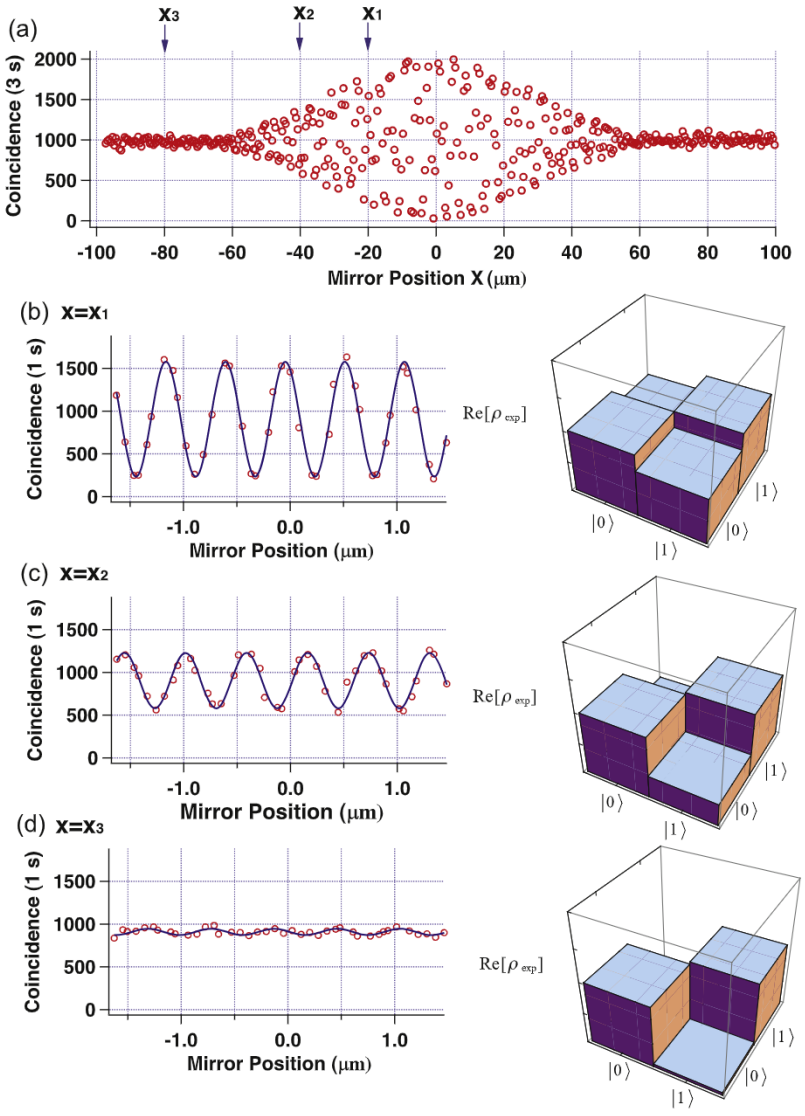

Fig. 5. Experimental data for mixed state path qubits with a HWP setting $\theta = 22.5°$. (a) First-order single-photon interference fringe observed at the signal detector. Arrows represent the mirror positions where the mixed state path qubits are prepared. The single-photon interference fringe and the experimentally reconstructed density matrix are shown for different mirror positions: (b) $x_1 = -10$ μm, (c) $x_2 = -40$ μm, (d) $x_3 = -80$ μm. The corresponding $Tr(\rho_{exp}^2)$ are 0.776, 0.564, and 0.501, respectively.

tained from the first-order single-photon quantum interference fringe. A set of six projection measurement outcomes allow full tomographic characterization of an arbitrary single-photon path qubit. Although, in this experiment, both the phase and purity (mixedness) adjustment were accomplished by moving one of the mirrors of the Mach–Zehnder interferometer, more precise phase control can be implemented with a rotatable quartz plate either in path-0 or in path-1 while the purity (mixedness) adjustment can be made with the larger mirror movement.

We note that the present protocol and scheme could be expanded to explore entanglement of multiple single-photon path qubits and high-dimensional path qudit states [40]. Our scheme will also find applications in preparation and measurement of the single-photon two-qubit entangle state [15–19] if the additional polarization degree of freedom is incorporated into the present setup.

Acknowledgements

This work was supported by the National Research Foundation of Korea (2009-0070668 and 2009-0084473) and the Ministry of Knowledge and Economy of Korea through the Ultrafast Quantum Beam Facility Program.

References

[1] M.A. Nielsen, I.L. Chuang, Quantum Computation and Quantum Information, Cambridge University Press, Cambridge, UK, 2000.
[2] E. Knill, R. Laflamme, G.J. Milburn, Nature 409 (2001) 46.
[3] P.G. Kwiat, E. Waks, A.G. White, I. Appelbaum, P.H. Eberhard, Phys. Rev. A 60 (1999) R773.
[4] N.J. Cerf, M. Bourennane, A. Karlsson, N. Gisin, Phys. Rev. Lett. 88 (2002) 127902.
[5] A. Mair, A. Vaziri, G. Weihs, A. Zeilinger, Nature 412 (2001) 313.
[6] R.T. Thew, A. Acín, H. Zbinden, N. Gisin, Phys. Rev. Lett. 93 (2004) 010503.
[7] A. Vaziri, G. Weihs, A. Zeilinger, Phys. Rev. Lett. 89 (2002) 240401.
[8] S.S.R. Oemrawsingh, A. Aiello, E.R. Eliel, G. Nienhuis, J.P. Woerdman, Phys. Rev. Lett. 92 (2004) 217901.
[9] N.K. Langford, R.B. Dalton, M.D. Harvey, J.L. O'Brien, G.J. Pryde, A. Gilchrist, S.D. Bartlett, A.G. White, Phys. Rev. Lett. 93 (2004) 053601.
[10] M.N. O'Sullivan-Hale, I. Ali Khan, R.W. Boyd, J.C. Howell, Phys. Rev. Lett. 94 (2005) 220501.
[11] L. Neves, G. Lima, J.G. Aguirre Gómez, C.H. Monken, C. Saavedra, S. Pádua, Phys. Rev. Lett. 94 (2005) 100501.

[12] G. Lima, L. Neves, I.F. Santos, J.G. Aguirre Gómez, C. Saavedra, S. Pádua, Phys. Rev. A 73 (2006) 032340.
[13] G. Lima, A. Vargas, L. Neves, R. Guzmán, C. Saavedra, Opt. Express 17 (2009) 10688.
[14] A. Rossi, G. Vallone, A. Chiuri, F.D. Martini, P. Mataloni, Phys. Rev. Lett. 102 (2009) 153902.
[15] Y.-H. Kim, Phys. Rev. A 67 (2003) 040301.
[16] B.-G. Englert, C. Kurtsiefer, H. Weinfurter, Phys. Rev. A 63 (2001) 032303.
[17] H.S. Park, J. Cho, J.Y. Lee, D.-H. Lee, S.-K. Choi, Opt. Express 15 (2007) 17960.
[18] G. Vallone, E. Pomarico, P. Mataloni, F. De Martini, V. Berardi, Phys. Rev. Lett. 98 (2007) 180502.
[19] S.-Y. Baek, Y.W. Cheong, Y.-H. Kim, Phys. Rev. A 77 (2008) 060308.
[20] P. Kalasuwan, G. Mendoza, A. Laing, T. Nagata, J. Coggins, M. Callaway, S. Takeuchi, A. Stefanov, J.L. O'Brien, J. Opt. Soc. Amer. B 27 (2010) A181.
[21] G. Lima, F. Torres-Ruiz, L. Neves, A. Delgado, C. Saavedra, S. Pádua, Opt. Commun. 281 (2008) 5058.
[22] G. Lima, F. Torres-Ruiz, L. Neves, A. Delgado, C. Saavedra, S. Pádua, J. Phys. B: At. Mol. Opt. Phys. 41 (2008) 185501.
[23] G. Taguchi, T. Dougakiuchi, N. Yoshimoto, K. Kasai, M. Iinuma, H.F. Hofmann, Y. Kadoya, Phys. Rev. A 78 (2008) 012307.
[24] G. Taguchi, T. Dougakiuchi, M. Iinuma, H.F. Hofmann, Y. Kadoya, Phys. Rev. A 80 (2009) 062102.
[25] G. Lima, L. Neves, R. Guzmán, E.S. Gómez, W.A.T. Nogueira, A. Delgado, A. Vargas, C. Saavedra, Opt. Express 19 (2011) 3542.
[26] M.A. Solís-Prosser, L. Neves, Phys. Rev. A 82 (2010) 055801.
[27] H. Bechmann-Pasquinucci, W. Tittel, Phys. Rev. A 61 (2000) 062308.
[28] M. Bourennane, A. Karlsson, G. Björk, Phys. Rev. A 64 (2001) 012306.
[29] N.J. Cerf, M. Bourennane, A. Karlsson, N. Gisin, Phys. Rev. Lett. 88 (2002) 127902.
[30] D. Aharonov, A. Kitaev, N. Nisan, ACM, 1998, p. 20.
[31] H. Barnum, C.M. Caves, C.A. Fuchs, R. Jozsa, B. Schumacher, Phys. Rev. Lett. 76 (1996) 2818.
[32] C.H. Bennett, D.P. DiVincenzo, J.A. Smolin, W.K. Wootters, Phys. Rev. A 54 (1996) 3824.
[33] M. Horodecki, P. Horodecki, R. Horodecki, Phys. Rev. Lett. 80 (1998) 5239.
[34] T.-C. Wei, K. Nemoto, P.M. Goldbart, P.G. Kwiat, W.J. Munro, F. Verstraete, Phys. Rev. A 67 (2003) 022110.
[35] D.F.V. James, P.G. Kwiat, W.J. Munro, A.G. White, Phys. Rev. A 64 (2001) 052312.
[36] S.-Y. Baek, S.S. Straupe, A.P. Shurupov, S.P. Kulik, Y.-H. Kim, Phys. Rev. A 78 (2008) 042321.
[37] C.K. Hong, L. Mandel, Phys. Rev. Lett. 56 (1986) 58.
[38] S.-Y. Baek, O. Kwon, Y.-H. Kim, Phys. Rev. A 77 (2008) 013829.
[39] S.-Y. Baek, O. Kwon, Y.-H. Kim, Phys. Rev. A 78 (2008) 013816.
[40] G. Weihs, M. Reck, H. Weinfurter, A. Zeilinger, Opt. Lett. 21 (1996) 302.